Calculating NMR Parameters in Aluminophosphates: Evaluation of Dispersion Correction Schemes

Scott Sneddon,[1] Daniel M. Dawson,[1] Chris J. Pickard[2] and Sharon E. Ashbrook[1]*

[1] *School of Chemistry and EaStCHEM, University of St Andrews, North Haugh, St Andrews KY16 9ST, UK*

[2] *Department of Physics and Astronomy, UCL, London, WC1E 6BT, UK*

*Author to whom correspondence should be addressed.

Email: *sema@st-andrews.ac.uk*

Submitted to *Phys. Chem. Chem. Phys.*

Abstract

Periodic density functional theory (DFT) calculations have recently emerged as a popular tool for assigning solid-state nuclear magnetic resonance (NMR) spectra. However, in order for the calculations to yield accurate results, accurate structural models are also required. In many cases the structural model (often derived from crystallographic diffraction) must be optimised (*i.e.*, to an energy minimum) using DFT prior to the calculation of NMR parameters. However, DFT does not reproduce weak long-range "dispersion" interactions well, and optimisation using some functionals can expand the crystallographic unit cell, particularly when dispersion interactions are important in defining the structure. Recently, dispersion-corrected DFT (DFT-D) has been extended to periodic calculations, to compensate for these missing interactions. Here, we investigate whether dispersion corrections are important for aluminophosphate zeolites (AlPOs) by comparing the structures optimized by DFT and DFT-D (using the PBE functional). For as-made AlPOs (containing cationic structure-directing agents (SDAs) and framework-bound anions) dispersion interactions appear to be important, with significant changes between the DFT and DFT-D unit cells. However, for calcined AlPOs, where the SDA/anion pairs are removed, dispersion interactions appear much less important, and the DFT and DFT-D unit cells are similar. We show that, while the different optimisation strategies yield similar calculated NMR parameters (providing that the atomic positions are optimised), the DFT-D optimisations provide structures in better agreement with the experimental diffraction measurements. Therefore, it appears that DFT-D calculations can, and should, be used for the optimisation of calcined and as-made AlPOs, in order to provide the closest agreement with all experimental measurements.

Keywords: DFT, semi-empirical dispersion correction, aluminophosphates, zeolites, solid-state NMR

Introduction

Recent advances in periodic approaches for the calculation of Nuclear Magnetic Resonance (NMR) parameters from first-principles have expanded the application of these methods among the experimental solid-state NMR community.[1-6] These calculations, typically exploiting density-functional theory (DFT), aid spectral assignment and interpretation, and can also predict NMR parameters and, therefore, guide experimental acquisition. For all calculations an initial structure (or structural model) is a vital pre-requisite, and this is usually obtained from experimental diffraction measurements or, alternatively, from computational studies. The accuracy of such structural models depends upon the exact type of diffraction that has been carried out, *i.e.*, single crystal or powder diffraction, whether laboratory X-ray, synchrotron X-ray or neutron diffraction have been used, and whether the positions of light atoms (in the case of X-ray diffraction) have been refined directly or have been added manually at a later stage. Furthermore, owing to the dependence of diffraction on long-range order in a solid, structural models derived solely in this way may need to be treated with some caution should there be any disorder or dynamics present, as only information on the average structure is obtained. In many cases, therefore, some optimisation of the structure is required, minimising the forces upon the atoms, prior to the calculation of NMR parameters. As NMR is an extremely sensitive probe of local structure, even small changes in the local geometry can have significant effects on the calculated NMR parameters.[5, 7-8]

Periodic DFT calculations have been used successfully to predict a range of physical and chemical properties for a variety of different materials.[2-6] However, traditional DFT calculations are not able to describe adequately long-range interactions in many systems, owing to the absence of van der Waals (vdW) forces in many exchange-correlation functionals, leading to possible inaccuracies in unit cell size and shape, and in the atomic coordinates of species within the cell.[9] While one might expect this to be less of a problem in densely-packed, rigid crystal lattices, it has been shown to be a considerable problem for the more flexible metal-organic frameworks (MOFs), where optimised structures can

differ significantly from the initial model.[10-11] For example, it was shown by Chang *et al.*, that optimisation of the structure of Zn(bpetpa) (a Zn-based MOF with 1,2-bis(4-pyridyl)ethane tetrafluoroterephthalate (bpetpa) linkers) using standard DFT calculations resulted in a considerable expansion of the unit cell size (~12.6% along the *b* axis).[11] Furthermore, many molecular crystals are bound by dispersion interactions, and their absence in any optimisation using DFT can either cause the structure simply to "fall apart" or the geometry (*i.e.*, the packing of molecules) to be significantly altered.[9] One solution to prevent unreasonable or unphysical expansion of the unit cell size is to constrain the lattice parameters, *i.e.*, the cell dimensions (*a*, *b*, *c*) and angles (α, β and γ) to those determined by diffraction. This is not, however, a particularly satisfying solution, as this assumes not only that the diffraction measurements are absolutely accurate (and complete), but that the "average" structure measured by diffraction at a finite temperature will be similar to the minimum energy structure at 0 K found using DFT. Furthermore, this approach will fail for systems where disorder (either compositional or positional) is present, with diffraction providing information only on an average structure (e.g., including atoms with fractional occupancies), while calculations are performed using a specific arrangement of atoms or molecules within the defined unit cell.

In recent years, a number of approaches have been developed to include dispersion interactions in DFT calculations,[9] including the development of hybrid density functionals, vdW-DFT[9, 12-13] and the use of use of semi-empirical dispersion correction (SEDC) schemes (or DFT-D).[14-16] In the latter case, the total energy of the system is modified by adding a contribution from an empirical dispersion correction to the value obtained using Kohn-Sham DFT. The schemes introduced by Grimme (G06)[14] and Tkatchenko and Scheffler (TS)[15] have both been shown to be compatible with periodic calculations performed using the generalised gradient approximation (GGA) PBE functional – a functional that has become a particularly popular choice for the calculation of NMR parameters in solids.[2-3, 6] Notably, the use of both corrections schemes for the structure optimisation of Zn(bpetpa) resulted in a structure in much better agreement with that from diffraction, matching all unit cell parameters to within 1.3%.[11]

Aluminophosphates (AlPOs) are an important class of microporous materials, with applications in gas storage and separation, catalysis and medicine. First reported in 1982, AlPOs have been widely studied owing to their structural similarity to zeolites, although materials with unique topologies can also be formed.[17-19] Conventionally, AlPOs are synthesised hydrothermally (or solvothermally) in the presence of a structure directing agent (SDA) or "template", usually an amine, which remains in the pores of the final product. Any charge on the SDA is balanced by the incorporation of OH^- or F^- anions, within the framework, resulting in four-, five- and six-coordinate framework Al species. Calcination (typically at 500-600 ºC) of the as-made form removes the SDA, any water contained within the pores and the charge-balancing OH^-/F^- anions, resulting in a tetrahedral framework containing corner-sharing AlO_4 and PO_4 units.[18-19] This change is shown in Figure 1, using the structures of as-made and calcined AlPO-14 as an example. The positive charges on the two isopropylammonium (ipa) SDA cations per pore are balanced by the incorporation of two OH^- groups into the framework structure, and there are also two water molecules found per pore.[20-21] Calcination produces a neutral, and purely tetrahedral, open framework structure. Substituted materials (referred to as MeAPOs, where Me = Metal) are commonly encountered, owing to enhanced catalytic properties, and the ability to "tune" the properties of the framework for a particular application.[18-19] NMR spectroscopy is a popular approach for studying AlPOs, as the main constituents of the pure and substituted frameworks ($^{27}Al/^{31}P/^{17}O$ and ^{25}Mg, ^{71}Ga, ^{29}Si, *etc.*,), the SDA ($^{13}C/^{1}H/^{15}N$) and the charge-balancing anions ($^{17}O/^{1}H/^{19}F$) are all NMR active. Furthermore, the sensitivity of NMR to the atomic-scale environment makes it an ideal probe for investigating the framework structure and (dis)order, the nature, position and dynamics of guest molecules within the pores, and the number and position of (potentially disordered) charge-balancing anions. In this respect, the ability to compare calculated NMR parameters to those obtained experimentally is invaluable in understanding possible local structural environments present, and periodic DFT calculations of NMR parameters have been successfully applied in the structural investigation of a number of phosphate-based frameworks.[2, 22-29]

Unlike many densely-packed, rigid crystalline materials, some flexibility of the AlPO framework structure is possible, with variations in symmetry, and pore size and shape upon the incorporation of guest molecules (be it the original SDA or one specifically loaded).[18-19] This flexibility, however, is not as great as that typically encountered in many MOFs, where significant structural changes are possible without breaking any chemical bonds.[19] The guest molecules present in AlPOs will interact with the framework, and with each other, through longer-range interactions. Therefore, it is not clear how the inclusion of dispersion corrections schemes into DFT calculations may affect the optimised structures and, ultimately, the accuracy of the calculated NMR parameters for these materials. In this work, we investigate how the structures of a range of as-made and calcined AlPOs vary when optimised using DFT with the inclusion of SEDC schemes. We compare the structures obtained using two such schemes, specifically G06 and TS, to that produced when no such contribution is included. Subsequently, we consider how the structural changes affect the calculated NMR parameters, comparing those calculated for the different structural models to experimental parameters present in the literature, in order to determine the optimum approach for carrying out this type of calculation.

Methods

Calculations of total energies and NMR parameters were carried out using the CASTEP DFT code (version 5.5.2),[30] employing the gauge-including projector augmented wave (GIPAW) approach,[1] to reconstruct the all-electron wavefunction in the presence of a magnetic field. Calculations were performed using the GGA PBE functional[31] and core-valence interactions were described by ultrasoft pseudopotentials.[32] A planewave energy cutoff of 50 Ry (~680 eV) was used, and integrals over the Brillouin zone were performed using a Monkhorst-Pack grid with a k-point spacing of 0.04 $Å^{-1}$. All calculations were converged as far as possible with respect to both k-point spacing and cutoff energy. Calculations were performed on a 198-node (2376 core) Intel Westmere cluster with 2 GB

memory per core and QDR Infiniband interconnect at the University of St Andrews. Calculation wallclock times ranged from 24 to 48 hours using 1-8 nodes.

Calculations generate the absolute shielding tensor ($\boldsymbol{\sigma}$) in the crystal frame, and diagonalisation yields the three principal components, σ_{XX}, σ_{YY} and σ_{ZZ}, and the isotropic shielding, $\sigma_{iso} = (1/3)\ \mathrm{Tr}\{\boldsymbol{\sigma}\}$. The isotropic chemical shift, δ_{iso}, is given by $-(\sigma_{iso} - \sigma_{ref})$, where σ_{ref} is a reference shielding. The quadrupolar coupling constant, $C_Q = eQV_{ZZ}/h$ and asymmetry parameter, $\eta_Q = (V_{XX} - V_{YY})/V_{ZZ}$ are obtained from the principal components of the electric field gradient (EFG) tensor, $\mathbf{V}$, where Q is the nuclear quadrupole moment (for which a value of 146.6 mB was used for ^{27}Al).[33] Although both the sign and magnitude of C_Q are generated, the latter is difficult to measure experimentally and so only the magnitude of C_Q is considered here.

Initial atomic positions and unit cell parameters were taken from the literature, and typically obtained from diffraction measurements. References and further details are given in the text. Optimisation of the structures was performed where necessary using BFGS optimisation with an energy cutoff of 50 Ry and a k-point spacing of 0.04 $Å^{-1}$. The convergence criteria for total energy, ionic force and ionic displacement were 1×10^{-4} eV/atom, 0.05 eV/Å and 1×10^{-3} Å, respectively.

For DFT-D calculations, the SEDC schemes of Grimme (G06)[14] and Tkatchenko and Scheffler (TS)[15] were employed.[34] For G06, the dispersion contribution to the energy is calculated as a series of pairwise vdW interactions between each of the atoms in the system as a function of their internuclear separation (using a potential that contains a number of empirical parameters).[9,14] This contribution is then added to the energy determined using Kohn-Sham DFT, to give a DFT-D (or dispersion-corrected) energy. The form of the potential describing the dispersion contribution to the energy is similar in the TS scheme, but first-principles methods were used to determine some of the parameters empirically fitted by Grimme.[9,15]

^{31}P MAS NMR spectra were acquired using a Bruker Avance III 600 MHz spectrometer equipped with a 14.1 T widebore magnet, at a Larmor frequency of 242.9 MHz. Samples were packed in conventional 4-mm ZrO_2 rotors and rotated at an MAS rate of 14 kHz. Chemical shifts are referenced to 85% H_3PO_4 for ^{31}P using BPO_4 (–29.6 ppm)[7] as a secondary reference. (Note there are at least two slightly different referencing schemes in common use in the literature for ^{31}P, and spectra were acquired in this work to ensure consistency). Where necessary, continuous wave (cw) ^{1}H decoupling was employed to improve spectral resolution, with a typical radiofrequency field strength ($\gamma B_1/2\pi$) of ~100 kHz. For AlPO-14, low-power cw ^{27}Al decoupling[35] was also employed (($\gamma B_1/2\pi$) of ~10 kHz). All spectra were acquired using a recycle interval of 30 s. Experimental isotropic chemical shifts extracted from the spectra are given in the ESI. For ^{27}Al, most NMR parameters (isotropic chemical shifts, quadrupolar coupling and asymmetry) were taken from a range of previous work in the literature, with references given in the text. For calcined AlPO-17 and calcined AlPO-18, MAS NMR spectra were acquired using Bruker Avance III 400 and 600 MHz spectrometers equipped with 9.4 T and 14.1 T widebore magnets, at Larmor frequencies of 104.3 MHz and 156.4 MHz, respectively. Samples were packed in conventional 4-mm ZrO_2 rotors and rotated at an MAS rate of 14 kHz. Chemical shifts are referenced 1 M $Al(NO_3)_3$ (aq). Triple-quantum MAS NMR experiments were carried out using a phase-modulated split-t_1 shifted-echo pulse sequence,[36] with the efficiency of the conversion of triple- to single-quantum coherences enhanced by the use of soft-pulse-added-mixing (SPAM).[37] The final (180°) pulse was chosen to be selective for the central transition. The scale in the indirect dimension is referenced according to the convention in Ref. 38. All spectra were acquired using a recycle interval of 1 s. Experimental spectra and extracted NMR parameters are given in the ESI.

Results and Discussion

As-prepared AlPOs

The structures of a series of as-made AlPOs, obtained from diffraction measurements, were taken from the literature (see ESI for further details). These include (i) AlPO-14,[21] (ii) AlPO-15,[39] (iii) JDF-2,[40] (iv) AlPO-34,[41] and (v) SIZ-4,[42] containing isopropylammonium, ammonium, methylammonium, morpholinum and dimethylimidazolium cations, respectively, as SDAs. Charge balancing is achieved by the incorporation of either hydroxide (i-iii) or fluoride (iv-v) anions. Water molecules are also present in the pores for AlPO-14(isopropylamimonium hydroxide)[21] and AlPO-15(ammonium hydroxide).[39] Note that AlPO-34(morpholinum fluoride) and SIZ-4(dimethylimidazolium fluoride) are isostructural after calcination, but owing to their different preparation methods (using hydrothermal and ionothermal synthesis, respectively), their as-made forms contain different SDAs.[41-42]

Prior to the calculation of NMR parameters from a structural model, it is usually necessary to "optimise" the geometry, *i.e.*, to minimise forces upon the atoms. Table 1 shows the different possible optimisation strategies used in this work. Structural optimisation can be particularly important for as-prepared AlPOs, where H atoms (on the SDA, H_2O and charge-balancing hydroxyls) are often added manually, rather than being refined directly. Table 2 shows the (average) magnitude of the forces calculated on each atom type for the structure of each AlPO taken directly from the literature, termed structure set [A]. For all AlPOs, no matter how the diffraction data has been collected, high forces (in most cases over 1 eV/Å) are observed for most atoms, suggesting that some optimisation of the structure is necessary. The lowest forces are observed for AlPO-15(ammonium hydroxide),[39] probably owing to the presence of a simpler SDA. Also shown in Table 2 are the magnitudes of the forces present after only H positions were optimised (with the coordinates of all other atoms and the unit cell size and shape fixed) – termed structure set [B]. It can be seen that optimisation has significantly reduced the forces on H and many of the nearby atoms, but that some high forces are still present. In all cases, however, optimisation has reduced the total energy (in most cases by a significant amount). If all atomic coordinates are optimised (with the unit cell size and

shape remaining fixed), as in structure set [C] in Table 2, the forces on each atom are now much lower (typically below 0.05 eV/Å), suggesting an energy minimum has been reached. (Note that in this case the optimisation was carried out from the initial structure [A] and not from the part-optimised structure [B].) The energies of each structure in set [C] are lower than the corresponding structures in set [A] and [B] in all cases. The optimisation resulted in only very small changes to the structure in most cases. As an example, in AlPO-34(morpholinum fluoride) changes in the atomic positions of atoms in the aluminophosphate framework of less than ~0.06 Å are observed, although larger changes (up to ~0.3 Å) are observed for the atoms in the morpholinum SDA. The SDA in this case is conformationally flexible and may be difficult to study using diffraction and, notably, the refined structure of the as-made material contains an unusual boat-like conformation for this molecule, rather than the chair-like confirmation observed after optimisation.

It is clear that optimisation of structural models from the literature is often necessary. However, for disordered materials, or those where the structure has been modified or altered in some way, fixing the unit cell size and shape is not necessarily an option (as the "true" values are not always known). In the case of disordered materials values obtained from diffraction are the result of averaging over many unit cells, and do not necessarily reflect the specific arrangement of atoms in the cell or supercell considered in the calculation for any structural model. In this case, it is necessary to allow the unit cell parameters (*i.e.*, the values of (*a*, *b*, *c*) and (α, β and γ)) to vary, along with the atomic coordinates. Table 2 shows that such an optimisation (structure set [D]) also results in small forces on the atoms, and typically a very small (*e.g.*, 0.1-0.5 eV/cell) lowering of the total energy. It is noticeable, however, that this optimisation has resulted in a change in the unit cell size and, to a lesser extent, its shape.

Figure 2a shows the (%) change in the unit cell dimensions and total volume between structure sets [A] and [D] for each as-made AlPO. (Full information on the change in the unit cell parameters for each AlPO is given in the ESI.) It can be seen that, in

all cases, varying the unit cell size and shape in the optimisation has resulted in a typical increase in the cell dimensions of ~1% (and an increase in volume of between 2 and 4 %). Notably, for JDF-2(methylammonium hydroxide) the expansion appears to be anisotropic, being much greater along the *b* axis than along either *a* or *c*. In general, the distance and volume increases observed are much smaller than those seen in previous work for the Zn(bpetpa) MOF (~12% volume change[11]), as a result of the much less flexible nature of the AlPO framework, although the possibility for atomic movement in these cases is significantly greater than in many rigid solids. These small differences in cell size/shape do, however, affect the observed diffraction pattern. An example of this is shown in Figure 3, where simulated powder X-ray diffraction patterns for the [A], [C] and [D] structures of JDF-2(methylammonium hydroxide), are compared. There are, of course, no differences in peak positions within the patterns for structures [A] and [C] as the unit cell size remains fixed. However, there are also no significant changes in the intensities of the peaks despite the changes in the atomic coordinates, suggesting that powder diffraction would be relatively insensitive to the small changes that have occurred. There are significant changes in some of the peak positions for structure [D], owing to the change in unit cell size upon optimisation (shown in Figure 2). It can be seen that (*h*0*l*) diffraction peaks are less affected, as expansion along the *a* and *c* axes is significantly less than that along *b*.

For all AlPO structures two additional optimisations were carried out with the inclusion of dispersion forces according to the G06 (structure set [E]) and TS schemes (structure set [F]). All atomic positions and the unit cell parameters were allowed to vary. Figures 2b and 2c show the change in the unit cell dimensions and total volume between structure sets [A] and [E] or [F], for each as-made AlPO. For each of the optimised structures, forces of similar magnitude to those for structure sets [C] and [D] were observed. (These are given in the ESI, as they are not directly comparable to those quoted in Table 2, owing to the different computational methods used). In general, the expansion in cell volume seen for structure set [D] is not observed, with all cells displaying a small contraction in volume, and a contraction is also observed along most individual axes. An exception to this is the expansion along the *b* axis (of ~1.65 %) observed for JDF-

2(methylammonium hydroxide), perhaps indicating some error in the initial diffraction measurement for this compound. With this exception, the cell size of the optimised structures obtained using SEDC schemes do appear to be in better agreement with the diffraction measurements, and this is reflected in greater similarity between experimental and simulated diffraction patterns shown in Figure 3.[40] It is possible that the small contractions that appear to be observed in most cases could be the result of "overbinding", *i.e.*, an overestimation of the dispersion forces by the correction schemes, but it is difficult to say this with any confidence as the "exact" answer is not known definitively. Figure 2 uses the diffraction measurements as a baseline for the comparison, but these are also, of course, subject to errors (both inherent, systematic and user related). It should also be noted that DFT calculations correspond to a 0 K structure, while experimental diffraction measurements will have been carried out at higher temperatures, which could contribute to the small contraction seen. The largest decrease in cell size is seen for AlPO-14(isopropylammonium hydroxide), for which significant dynamics on the μs timescale have been observed in previous work.[43] It is also worth noting that the results obtained using G06 and TS correction schemes are generally very similar, suggesting that if any inherent errors are present they would appear to be similar for the two approaches.

NMR parameters were then calculated for both the original and optimised structures. Figure 4 plots calculated and experimental ^{31}P and ^{27}Al NMR parameters for all as-made AlPOs. For ^{31}P, MAS NMR spectra were recorded as described in the experimental section (to ensure a consistent referencing scheme) and the extracted isotropic shifts are shown in the ESI. For ^{27}Al, NMR parameters were taken from Refs. 22, 25, 24, 44 and 27 for AlPO-14, AlPO-15, JDF-2, AlPO-34 and SIZ-4, respectively, where they have typically been determined using a variety of experimental approaches at multiple fields. As expected, a negative correlation is observed between calculated shielding and experimental shift (a deshielding parameter), with a gradient close to 1 for both ^{31}P and ^{27}Al. Interestingly, for ^{31}P the gradient is slightly below –1 for each structure set, while for ^{27}Al it is slightly above, indicating a small overestimation and underestimation, respectively, in the calculated values. However, the relatively small

number of data points considered here precludes any fundamental conclusions of the accuracy of the DFT calculations for Al or P. It is clear for both nuclei that agreement between experiment and calculation for the shielding is poorer for the unoptimised structures, with the increased scatter being reflected in a lower regression coefficient, R^2. The reference shielding, σ_{ref}, (needed to convert the calculated shielding σ_{iso} to a calculated shift δ_{iso}) can be determined from the intercept of the plot. Similar results are observed for structure set [B], despite the lowering of the overall energy and the lower forces observed on some of the atoms shown in Table 2. An improvement is clear, however, in any structure set where all atomic positions are varied, *i.e.*, sets [C]-[F], irrespective of whether the cell itself is fixed or variable and whether or not SEDC schemes are employed. A very similar result is observed for ^{27}Al, although the plots are dominated by the much larger changes in chemical shift resulting from the change in coordination number associated with the coordination of charge-balancing anions to the framework, giving four- (δ_{iso} of 40 to 50 ppm), five- (δ_{iso} of 15 to 25 ppm) and six-coordinate (δ_{iso} of –5 to 5 ppm) Al species.[7] It should also be noted that due to the presence of second-order quadrupolar broadening in the ^{27}Al MAS NMR spectra, there may be a higher uncertainty associated with the experimental values for this nucleus than for ^{31}P.

When the ^{27}Al quadrupolar coupling constant is considered, it can be seen that the agreement with experiment is considerably poorer for the unoptimised structures (R^2 = 0.787), with some improvement observed upon optimisation of only H positions. Best agreement is obtained for structure set [D] where the cell size has varied during the optimisation although the differences in regression parameters are quite small. As described above, however, it can be significantly more difficult to determine quadrupolar coupling constants very accurately by experiment, particularly when C_Q is low and lineshapes are broadened by any disorder/dynamics in the system, leading to much greater uncertainty in the experimental measurements.

In general, much better agreement between experimental and calculated NMR parameters is obtained after optimisation has been carried out. It is interesting to note,

however, that the changes in the atomic coordinates between structure sets [A] and [C], that had no noticeable affect on the diffraction patterns for this material (shown in Figure 3), do have a significant effect upon the NMR parameters. However, these parameters appear much less sensitive to the small changes in unit cell size/shape (or the use of SEDC schemes) once structures have been optimised. If SEDC schemes are included, similar results are usually obtained for both G06 and TS schemes, showing both are equally applicable for these inorganic periodic solids. As an example, Figure 5 shows how the local structure, *e.g.*, bond angles and bond distances, in AlPO-14(isopropylammonium hydroxide)[21] vary as differing optimisations are performed. Relatively small changes are observed in the Al-O and P-O bond distances between the optimised structures [C-F], although changes in the average <Al-O> and <P-O> distances for any one species are smaller still (~0.006 Å and 0.002 Å for Al and P, respectively). However, the differences between the NMR parameters for unoptimised [A] and optimised [C-F] structures are often much greater (~0.014 Å (<Al-O>) and 0.015 Å (<P-O>)). It has been shown in previous literature that isotropic chemical shifts (particularly for ^{31}P) show a dependence on the <P-O-Al> angle.[45-47] Figure 5c shows that the largest changes in P-O-Al angles for AlPO-14(isopropylammonium hydroxide) usually occur between [A] and [C-F], *i.e.*, upon initial optimisation, although changes in the average <P-O-Al> angle are generally smaller (~3°, predicted to correspond to a change of 2.5 - 4 ppm in the ^{31}P chemical shift[45-47]). Clearly the small changes observed in the local structure between the sets of optimised structures produce relatively small changes in the NMR parameters. These parameters are however, more sensitive to the larger changes that occur upon any optimisation of the initial structural model.

Calcined AlPOs

Neutral tetrahedral AlPO frameworks can be obtained after calcination, which removes the SDA, charge-balancing anions and any water contained within the pores. It might be expected that as these simpler materials should be more easily and accurately characterised using diffraction methods, and that dispersion interactions may well be of

less importance. However, the flexible nature of the structure in comparison to simpler, more rigid inorganic solids does still require the optimal computational approach to be determined. The structures of a series of calcined AlPOs ((i) AlPO-14,[20] (ii) AlPO-53(B),[48] (iii) AlPO-34,[49] (iv) AlPO-17[50] and (v) AlPO-18[51] were obtained from the literature (see ESI for further details)). The structures of as-made AlPO-17[52] and AlPO-18[51] have been reported in the literature, with piperidinium and tetraethylammonium, respectively as the SDA, but the crystal structures exhibit considerable disorder in the SDA position and so these materials were not discussed with the other as-made AlPOs above. Calcination of both AlPO-34(morpholinum fluoride) and SIZ-4(dimethylimidazolium fluoride) produce AlPO-34,[41,42] while calcination of JDF-2(methylammonium hydroxide) produces AlPO53(B).[24,48] It is not possible to calcine AlPO-15(ammonium hydroxide), as this material decomposes at 300°C.[53] In general, calcination of AlPOs produces significant changes in the local geometry of the framework atoms, and often results in increased symmetry compared to the as-made materials. These changes can have a significant impact upon NMR spectra. The reduction in disorder can make spectra considerably less complicated, with fewer overlapping lineshapes, but the species present are usually much more similar to each other (both in their local geometry and resulting NMR parameters), hindering spectral assignment and requiring accurate DFT calculations to be performed to achieve a reliable assignment.

Table 3 shows the (average) magnitude of the forces calculated on each atom type for the structure of each calcined AlPO taken directly from the literature (structure set [A]). High forces (in most cases over 1 eV/Å) are observed for most materials, despite the simpler structures, the lack of any templates, charge-balancing anions or the manual determination of any H positions, suggesting structural optimisation is required. Forces are considerably smaller when atomic coordinates have been optimised (with either fixed or variable cell parameters – sets [C] and [D], respectively), and the energy is also lower in all cases. Figure 6a shows the (%) change in the unit cell dimensions and total volume between structure sets [A] and [D] for each calcined AlPO. (Full information on the change in the unit cell parameters is given in the ESI.) In all cases an increase in the unit cell size is

observed (typically of ~1% along each dimension, and ~3% in the volume), and is of a similar magnitude in all dimensions. These changes are similar to those observed for the as-made AlPOs, and were shown above to have a noticeable effect upon the predicted diffraction pattern.

For all calcined AlPOs two additional optimisations were carried out with the inclusion the G06 and TS SEDC schemes (structure sets [E] and [F], respectively), with all atomic positions and the unit cell size and shape allowed to vary. For each of the optimised structures, forces of similar magnitude to those for structure sets [C] and [D] were observed (see ESI). Changes in the unit cell dimensions and total volume between structure sets [A] and [E] or [F] are shown in Figures 6b and 6c, respectively. In contrast to the changes seen for as-made AlPOs (Figure 2), in all cases, an expansion of the unit cell is still seen, though this is typically smaller than that for structure set [D]. As discussed above, it is difficult to draw completely unambiguous conclusions from Figure 6, owing to the small number of systems studied and the uncertainty associated with the accuracy of the initial diffraction measurements; however, it would seem that the effect of dispersion forces on the structure of calcined AlPOs is much less significant, with only small changes observed when SEDC schemes are employed. Application of the G06 and TS SEDC schemes produced very similar results in all cases. For as-made AlPOs, a contraction of the unit cell size was observed upon the use of SEDC schemes, and while it was noted that this could result from overbinding, the possibility of a thermal contraction (from higher temperature experimental measurements) was also discussed. In light of the latter point it is interesting to note that calcined AlPO-17, AlPO-18 and AlPO-34 have all been observed to display negative thermal expansion behaviour,[49-51] which would be expected to result in an expansion of the cell length in a 0 K structure, relative to an experimental measurement at higher temperature. Figure 6, therefore, suggests that AlPO-53(B) and AlPO-14 may also display negative thermal expansion behaviour and points to possible future investigation.

Figure 7 plots calculated and experimental ^{31}P and ^{27}Al NMR parameters for all calcined AlPOs. For both ^{31}P and ^{27}Al isotropic shifts, poor correlation is observed between

experiment and calculation before optimisation, with similar accuracy observed for optimised structure sets [C-F]. At first sight the agreement with experiment seems poorer than that obtained for the as-made AlPOs, but the range of shifts considered is much smaller, *i.e.*, species are generally more similar. Interestingly, as observed for as-made AlPOs the gradient of the line of best fit is slightly below –1 for ^{31}P, and slightly above for ^{27}Al. (Note once again the difficulty in extracting accurate experimental isotropic shifts for ^{27}Al owing to the presence of quadrupolar broadening.) Good agreement is observed for the ^{27}Al quadrupolar interaction between experiment and calculation for all optimised structure sets, although poor results are obtained prior to any optimisation. For all parameters, very little difference is observed between structure sets [C-F], *i.e.*, upon the inclusion of SEDC schemes, suggesting these can be included with no detrimental effects upon the final results. Little difference is observed between the G06 and TS approaches. This can also be seen in Figure 8, where experimental spectra of calcined AlPO-14 are compared to those simulated using the parameters calculated with DFT for the varying structure sets. The spectra obtained prior to optimisation are in very poor agreement with the experimental measurements, with a very different assignment of the ^{31}P spectrum, and very broad lineshapes (owing to the very large quadrupolar couplings) observed for ^{27}Al. Much better agreement with the experimental spectra is obtained when the structures are optimised, with spectra for structures [E] and [F] producing very similar results. Note that in order to compare experimental and calculated spectra it is also necessary to convert the calculated shielding to a calculated shift using a reference shielding. For each optimisation method, the reference used is that obtained from the corresponding plot in Figure 7, *i.e.*, slightly different reference shieldings are used for each optimisation method. Given the poor correlation between experiment and calculation for structure set [A], an inaccurate reference value is obtained. Therefore, a second simulated spectrum is also shown (in red) for [A], where the reference value for structure set [C] has been used.

The similarity in the NMR parameters for structure sets [C-F] can once again be explained by considering the local structure in these materials. As Figure 9 shows for calcined AlPO-14, there are very small changes in local structure between the optimised

structure sets [C-F], with maximum changes of 0.004 and 0.007 Å for P-O and Al-O bond distances, respectively. However, much more significant changes are observed between the initial structure and the optimised structures, particularly in the bond distances, with maximum changes of 0.13 Å (P-O) and 0.12 Å (Al-O). It is noticeable that in this particular case, optimisation has resulted in more similar bond distances for any one tetrahedral Al/P species. In general, the results observed are very similar to those for the as-made materials, with only small changes seen in the local structure between differing optimisation methods, producing very similar NMR parameters in all cases, but a much greater change upon any optimisation of the initial structural model.

Conclusions

We have shown that optimisation of the structure of both as-made and calcined AlPOs can lead to a significant improvement in the calculated ^{27}Al and ^{31}P NMR parameters, owing to small changes in the local environment of the Al and P species. However, the precise optimisation strategy chosen can also alter the agreement of the structure with the experimental diffraction measurements from which the initial structural model is typically derived. If the diffraction measurements are assumed to be exactly correct, the average unit cell obtained from diffraction can be retained throughout the structural optimisation. However, this is clearly not an option for disordered systems, where optimisation of the unit cell is essential for a given structural model, as the specific arrangement of atoms considered cannot correspond to the average structural picture determined by diffraction. Traditional DFT calculations do not include a description of the weak, long-range dispersion interactions such as vdW forces, meaning that, where such interactions contribute significantly to the system, their omission can lead to an expansion of the unit cell in the structural optimisation using some functionals if this is not fixed. We observed an average expansion of ~2.7% in the unit cell volume for as-made AlPOs, indicating that dispersion interactions appear to be significant in determining the unit cell parameters, with the optimised structures giving very poor agreement with the experimental diffraction patterns. However, despite this discrepancy between the

experimental and calculated diffraction patterns, the experimental and calculated NMR parameters are in similar (or typically slightly better) agreement with the experimental results than when the cell size is fixed.

Dispersion-corrected DFT (DFT-D) calculations are a relatively new means of overcoming the unit cell expansion by including a semi-empirical correction term to the calculated energy of the system and allowing for a more realistic structure to be obtained upon optimisation. The use of either the G06 or TS SEDC schemes in the optimisation of as-made AlPOs yielded much closer agreement with the experimental diffraction measurements, with a small contraction of the unit cell volume observed upon optimisation. This can possibly be attributed to slight "overbinding" of the SEDC schemes, but may also be related to either errors in the diffraction measurements, or the fact that the DFT calculations are carried out at 0 K, whereas the diffraction measurements are carried out at higher temperature and might, therefore, include some contribution from the thermal expansion of the unit cell, which may be more significant for these open framework materials than for denser, more rigid solids.

Thermal effects may be particularly relevant for AlPOs, as many calcined AlPOs have been shown to display negative thermal expansion behaviour. Indeed, optimisation revealed that the unit cells of all calcined AlPOs studied here expanded (by ~1.4 to 3.3%) regardless of the optimisation method used (although larger expansions were typically observed when dispersion corrections schemes were not used). This suggests that (a) dispersion interactions play a much smaller role in the structure of calcined AlPOs (as may be expected, given the SDA/anion pair is absent) and (b) negative thermal expansion may lead to this discrepancy between the diffraction structure (obtained at finite temperature) and the DFT and DFT-D structures (nominally at 0 K). It is interesting to note that the negative thermal expansion properties of two of the calcined AlPOs studied in this work, AlPO-14 and AlPO-53(B), are predicted from the results of the DFT and DFT-D calculations reported here, but have not yet been investigated experimentally in this respect.

The structural optimisation method is, therefore, clearly important in order to achieve a reasonable agreement with the experimental diffraction measurements (when smaller thermal expansion/contraction effects are taken into account). However, we have shown that there is reasonable agreement between the calculated and experimental NMR parameters for all optimised structures (though agreement is often quite poor if no optimisation is used). This reflects the sensitivity of the NMR parameters to the local structure, rather than the precise size and shape of the longer-range periodic repeat unit. However, as the computational cost of the DFT-D calculations is essentially the same as the DFT calculations, while the former gives much better agreement with the experimental diffraction experiments, it would seem that the use of DFT-D schemes during optimisation for all AlPOs will give reliable values for both the atomic coordinates and the unit cell size and shape, as well as the NMR parameters.

Acknowledgements

We would like to thank EPSRC (EP/E041825/1, EP/J501542/1 and EP/J010510/1) for support, for the award of studentships to SS and DMD and a fellowship to CJP. We thank EaStCHEM for computational support through the EaStCHEM Research Computing Facility. Professor Richard Walton (University of Warwick) and Dr John Griffin are thanked for providing some of the AlPO samples used in this work.

Electronic Supplementary Information (ESI) available: Experimental ^{31}P (all materials) and ^{27}Al (calcined AlPO-17 and AlPO-18 only) NMR parameters, initial structural models, unit cell parameters pre and post DFT optimisation, and ionic forces for structural models optimised using dispersion correction schemes, for as-made and calcined AlPOs. All calculated data is available from the authors upon request.

Table 1. Labels used for different optimisation strategies in this work.

Structure set	Optimisation Strategy
[A]	No optimisation of initial structure
[B]	Optimisation of H atomic coordinates
[C]	Optimisation of all atomic coordinates with fixed cell size and shape
[D]	Optimisation of all atomic coordinates and cell size and shape
[E]	Optimisation of all atomic coordinates and cell size and shape, using G06 SEDC scheme
[F]	Optimisation of all atomic coordinates and cell size and shape, using TS SEDC scheme

Table 2. Average magnitude of the forces (in eV/Å) upon each atom type, and total energies (in eV), for structural models of a range of as-made AlPOs, pre and post DFT optimisation.

	Ionic forces /(eV/Å)				
	AlPO-14[21]	AlPO-15[39]	JDF-2[40]	AlPO-34[41]	SIZ-4[42]
[A] Initial structure from diffraction literature					
H	7.30	1.52	3.28	6.55	5.87
C	5.30		4.90	5.42	5.53
N	8.34	0.34	4.90	9.79	1.29
O	1.56	0.20	0.60	1.19	0.29
Al	1.21	0.07	0.23	0.91	0.11
P	1.56	0.14	0.29	2.54	0.24
F				0.30	0.33
Energy / eV	–20623.63	–23933.07	–58762.13	–16597.56	–16997.12
[B] After optimisation of atomic coordinates of H					
H	0.02	0.02	0.01	0.02	0.01
C	3.12		0.06	2.00	0.71
N	1.22	0.08	0.06	0.79	1.08
O	1.04	0.13	0.50	1.18	0.27
Al	0.75	0.12	0.13	0.86	0.12
P	1.75	0.26	0.31	2.49	0.20
F				0.34	0.29
Energy / eV	–20638.89	–23934.14	–58771.17	–16605.23	–17002.91
[C] After optimisation of all atomic coordinates					
H	0.02	0.01	0.03	0.02	0.01
C	0.01		0.04	0.01	0.01
N	0.02	0.01	0.04	0.02	0.01

O	0.01	0.01	0.02	0.02	0.02
Al	0.01	0.01	0.01	0.02	0.02
P	0.01	0.01	0.02	0.01	0.01
F				0.01	0.02
Energy / eV	–20641.16	–23934.20	–58771.79	–16607.86	–17003.04

[D] After optimisation of all atomic coordinates and unit cell parameters

H	0.02	0.02	0.01	0.01	0.01
C	0.01		0.01	0.01	0.02
N	0.03	0.03	0.01	0.01	0.01
O	0.02	0.02	0.02	0.01	0.02
Al	0.01	0.03	0.02	0.01	0.02
P	0.01	0.02	0.01	0.01	0.02
F				0.02	0.01
Energy / eV	–20641.25	–23934.32	–58772.31	–16607.97	–17003.19

Table 3. Average magnitude of the forces (in eV/Å) upon each atom type, and total energies (in eV), for structural models of a range of calcined AlPOs, pre and post DFT optimisation.

	Ionic forces /(eV/Å)				
	AlPO-14[20]	AlPO-53(B)[48]	AlPO-34[49]	AlPO-17[50]	AlPO-18[51]
[A] Initial structure from diffraction literature					
O	2.11	1.51	1.21	1.64	1.36
Al	1.31	1.54	0.52	0.48	1.29
P	2.73	3.53	2.11	0.76	1.34
Energy / eV	–16962.25	–50890.22	–38170.27	–38169.09	–50892.28
[C] After optimisation of all atomic coordinates					
O	0.02	0.02	0.02	0.03	0.02
Al	0.01	0.01	0.02	0.02	0.03
P	0.02	0.01	0.02	0.02	0.02
Energy / eV	–16964.95	–50895.58	–38171.78	–38171.48	–50895.65
[D] After optimisation of all atomic coordinates and unit cell parameters					
O	0.02	0.01	0.02	0.03	0.01
Al	0.02	0.01	0.01	0.02	0.02
P	0.02	0.01	0.01	0.02	0.02
Energy / eV	–16965.04	–508906.00	–38172.02	–38171.92	–50895.98

References

1. C. J. Pickard and F. Mauri, *Phys. Rev. B*, 2001, **63**, 245101.

2. C. Bonhomme, C. Gervais, F. Babonneau, C. Coelho, F. Pourpoint, T. Azaïs, S. E. Ashbrook, J. M. Griffin, J. R. Yates, F. Mauri, and C. J. Pickard, *Chem. Rev.*, 2012, **112**, 5733.

3. T. Charpentier, *Solid State Nucl. Magn. Reson.,* 2011, **40**, 1.

4. J. Cuny, S. Messaoudi, V. Alonzo, E. Furet, J. F. Harlet, E. L. Fur, S. E. Ashbrook, C. J. Pickard, R. Gautier and L. le Polles, *J. Comput. Chem.*, 2008, **29**, 2279.

5. S. E. Ashbrook and D. M. Dawson, *Acc. Chem. Res.*, 2013, **46**, 1964.

6. J. R. Yates and C. J. Pickard, Computations of Magnetic Resonance Parameters for Crystalline Systems: Principles, eMagRes, 2008 (DOI: 10.1002/9780470034590.emrstm1009).

7. K. J. D. MacKenzie and M. E. Smith, *Multinuclear Solid-State NMR of Inorganic Materials*, Pergamon Press, Oxford, 2002.

8. D. C. Apperley, R. K. Harris and P. Hodgkinson, *Solid State NMR Basic Principles and Practice,* Momentum Press, New York, 2012.

9. J. Klimeš and A. Michaelides, *J. Chem. Phys.*, 2012, **137**, 120901.

10. A. M. Walker, B. Civalleri, B. Slater, C. Mellot-Drazineks, F. Coirà, C. M. Zicovich-Wilson, G. Román-Pérez, J. M. Soler and J. D. Gale, *Angew. Chem. Int. Ed.* 2010, **49**, 7501.

11. K. Chang, P. D. Bristowe and A. K. Cheetham, *Phys. Chem. Chem. Phys.*, 2012, **14**, 7059.

12. M. Dion, H Rydberg, E. Schröder, D. C. Langreth and B. I. Lundqvist, *Phys. Rev. Lett.*, 2004, **92**, 246401.

13. K. Lee, É. D. Murray, L. Kong, B. I. Lundqvist and D. C. Langreth, *Phys. Rev. B,* 2010, **82**, 081101.

14. S. Grimme, *J. Comput. Chem.*, 2006, **27**, 1787.

15. A. Tkatchenko and M. Scheffler, *Phys. Rev. Lett.*, 2009, **102**, 073005.

16. F. Ortmann, F. Bechstedt and W. G. Schmidt, *Phys. Rev. B.*, 2006, **73**, 205101.

17. S. T. Wilson, B. M. Lok, C. A. Messina, T. R. Cannan and E. M. Flanigen, *J. Am. Chem. Soc.* 1982, **104**, 1446.

18. J. Yu and R. Xu, *Chem. Soc. Rev.*, 2006, **35**, 593.

19. P. A. Wright, *Microporous Framework Solids*, RSC Publishing, Cambridge, 2008.

20. R. W. Broach, S. T. Wilson and R. M. Kirchner, in *Proceedings of the 12th International Zeolite Conference*, ed. M. M. J. Treacy, B. C. Marcus, M. E. Bisher and J. B. Higgins, Materials Research Society, Warrendale, 1999, vol. 3, p. 1715.

21. R. W. Broach, S. T. Wilson and R. M. Kirchner, *Micropor. Mespor. Mater.*, 2003, **57**, 211.

22. S. E. Ashbrook, M. Cutajar, C. J. Pickard, R. I. Walton and S. Wimperis, *Phys. Chem. Chem. Phys.*, 2008, **10**, 5754.

23. Z. Han, A. L. Picone, A. M. Z. Slawin, V. R. Seymour, S. E. Ashbrook, W. Zhou, S. P. Thompson, J. E. Parker and P. A. Wright, *Chem. Mater.*, 2010, **22**, 338.

24. S. E. Ashbrook, M. Cutajar, J. M. Griffin, Z. A. D. Lethbridge, R. I. Walton and S. Wimperis, *J. Phys. Chem. C*, 2009, **113**, 10780.

25. P. J. Byrne, J. E. Warren, R. E. Morris and S. E. Ashbrook, *Solid State Sci.*, 2009, **11**, 1001.

26. M. Amri, S. E. Ashbrook, D. M. Dawson, J. M. Griffin, R. I Walton and S. Wimperis, *J. Phys. Chem. C*, 2012, **116**, 15048.

27. J. M. Griffin, L. Clark, V. R. Seymour, D. W. Aldous, D. M. Dawson, D. Iuga, R. E. Morris and S. E Ashbrook, *Chem. Sci.*, 2012, **3**, 2293.

28. M. Castro, V. R. Seymour, D. Carnevale, J. M. Griffin, S. E. Ashbrook, P. A. Wright, D. C. Apperley, J. E. Parker, S. P. Thompson, P. Stephen, A. Fecant, N. Bats, *J. Phys. Chem. C*, 2010, **114**, 12698.

29. V. R. Seymour, E. C. V. Eschenroeder, M. Castro, P. A. Wright and S. E. Ashbrook, *CrystEngComm*, 2013, **15**, 8668.

30. M. D. Segall, P. J. D. Lindan, M. J. Probert, C. J. Pickard, P. J. Hasnip, S. J. Clark and M. C. Payne, *J. Phys.: Condens. Matter*, 2002, **14**, 2717.

31. J. P. Perdew, K. Burke and M. Ernzerhof, *Phys. Rev. Lett.*, 1996, **77**, 3865.

32. J. R. Yates, C. J. Pickard and F. Mauri, *Phys. Rev. B*, 2007, **76**, 024401.

33. P. Pyykkö, *Mol. Phys.*, 2008, **106**, 1965.

34. E. R. McNellis, J. Meyer and K. Reuter, *Phys. Rev. B*, 2009, **80**, 205414.

35. L. Delevoye, C. Fernandez, C. M. Morais, J. P. Amoureux, V. Montouillout and J. Rocha, *Solid State Nucl. Magn. Reson.*, 2002, **22**, 501.

36. S. P. Brown and S. Wimperis, *J. Magn. Reson.*, 1997, **124**, 279.

37. T. J. Ball and S. Wimperis, *J. Magn. Reson.*, 2007, **187**, 343.

38. K. J. Pike, R. Malde, S. E. Ashbrook, J. McManus and S. Wimperis, *Solid State Nucl. Magn. Reson.*, 2000, **16**, 203.

39. E. Aubert, F. Porcher, M. Souhassou and C. Lecomte, *Acta. Crystallogr.*, 2003, **B59**, 687.

40. A. M. Chippindale, A. V. Powell, R. H. Jones, J. M. Thomas, A. K. Cheetham, Q. Huo, R. Xu, *Acta. Crystallogr.*, 1994, **C50**, 1537.

41. M. M. Harding and B. M. Kariuki, *Acta. Crystallogr.*, 1994, **C50**, 852.

42. E. R. Parnham and R. E. Morris, *Chem. Mater*. 2006, **18**, 4882.

43. S. Antonijevic, S. E. Ashbrook, S. Biedasek, R. I. Walton, S. Wimperis and H. Yang, *J. Am. Chem. Soc.*, 2006, **128**, 8054.

44. J. M. Griffin, personal communication.

45. D. Müller, E. Jahn, G. Ladwig and U. Haubenreisser, *Chem. Phys. Lett*. 1984, **109**, 332.

46. K. Kanehashi, T. Nemoto, K. Saito, *J. Non-Cryst. Solids*, 2007, **353**, 4227.

47. D. M. Dawson, PhD thesis, University of St Andrews, 2013.

48. R. M. Kirchner, R. W. Grosse-Kunstleve, J. J. Pluth, S. T. Wilson, R. W. Broach and J. V. Smith, *Micropor. Mesopor. Mater.*, 2003, **39**, 319.

49. M. Amri and R. I. Walton, *Chem. Mater.*, 2009, **21**, 3380.

50. M. P. Attfield and A. W. Sleight, *Chem. Mater.*, 1998, **10**, 2013.

51. A. Simmen, L. B. McCusker, Ch. Baerlocher and W. M. Meier, *Zeolites*, 1991, **11**, 654.

52. U. Lohse, E. Löffler, K. Kosche, J. Jänchen and B. Parlitz, *Zeolites*, 1993, **13**, 549.

53. D. E. W. Vaughan, H. P. Yennawar and A. J. Perrotta, *Micropor. Mesopor. Mater.*, 2012, **153**, 18.

Figure Captions

Figure 1. Structure of (a) as-made and (b) calcined AlPO-14. The as-made material contains the SDA (isopropylammonium) and water within the pores, and charge-balancing OH^- attached to the framework, creating four-, five- and six-coordinate Al species. Calcination produces a neutral, and purely tetrahedral, open framework structure.

Figure 2. Change (expressed as a %) in the unit cell dimensions and total volume between the unoptimised structure ([A]) and optimised structure sets (a) [D], (b) [E] and (c) [F] for a range of as-made AlPOs. See Table 1 for a description of each structure set.

Figure 3. Simulated powder X-ray diffraction patterns (Cu $K_{\alpha 1}$ radiation) for different structural models of JDF-2(methylammonium hydroxide). See Table 1 for a description of each structure set. The red dotted lines are included as a guide to the change in position of selected diffraction maxima.

Figure 4. Plot of (a) ^{31}P and (b) ^{27}Al calculated chemical shielding and experimental isotropic chemical shift, and (c) calculated and experimental ^{27}Al quadrupolar coupling constants. In (a, b), the subscript "iso" has been removed for clarity. Note in (c), only the magnitude of C_Q is considered, owing to the difficulty in measuring the sign of this quantity experimentally.

Figure 5. Plots showing how the local geometry ((a) Al-O bond distance, (b) P-O bond distance and (c) P-O-Al bond angles) varies between the different structure sets (described in Table 1) for AlPO-14(isopropylammonium hydroxide).

Figure 6. Change (expressed as a %) in the unit cell dimensions and total volume between the unoptimised structure ([A]) and optimised structure sets (a) [D], (b) [E] and (c) [F] for calcined AlPOs. See Table 1 for a description of each structure set.

Figure 7. Plot of (a) ^{31}P and (b) ^{27}Al calculated chemical shielding and experimental isotropic chemical shift, and (c) calculated and experimental ^{27}Al quadrupolar coupling constants, C_Q. In (a, b), the subscript "iso" has been removed for clarity. Note in (c), only the magnitude of C_Q is considered, owing to the difficulty in measuring the sign of this quantity experimentally.

Figure 8. Experimental and simulated (using the CASTEP calculated values) (a) ^{31}P and (b) ^{27}Al MAS NMR spectra of calcined AlPO-14. The reference shielding used for each set of structural models is that obtained from the corresponding plot in Figure 7. For structure set [A], a second spectrum is also shown (in red) using the reference value for structure set [C] owing to the poor correlation (and inaccurate reference value) obtained in Figure 7. For simulated spectra the (integrated) relative intensities of the spectral resonances reflect the proportion of the crystallographically-distinct sites in the material. † denotes a satellite transition in the experimental spectrum.

Figure 9. Plots showing how the local geometry ((a) Al-O bond distance, (b) P-O bond distance and (c) P-O-Al bond angles) varies between the different structure sets (described in Table 1) for calcined AlPO-14.

Figure 1

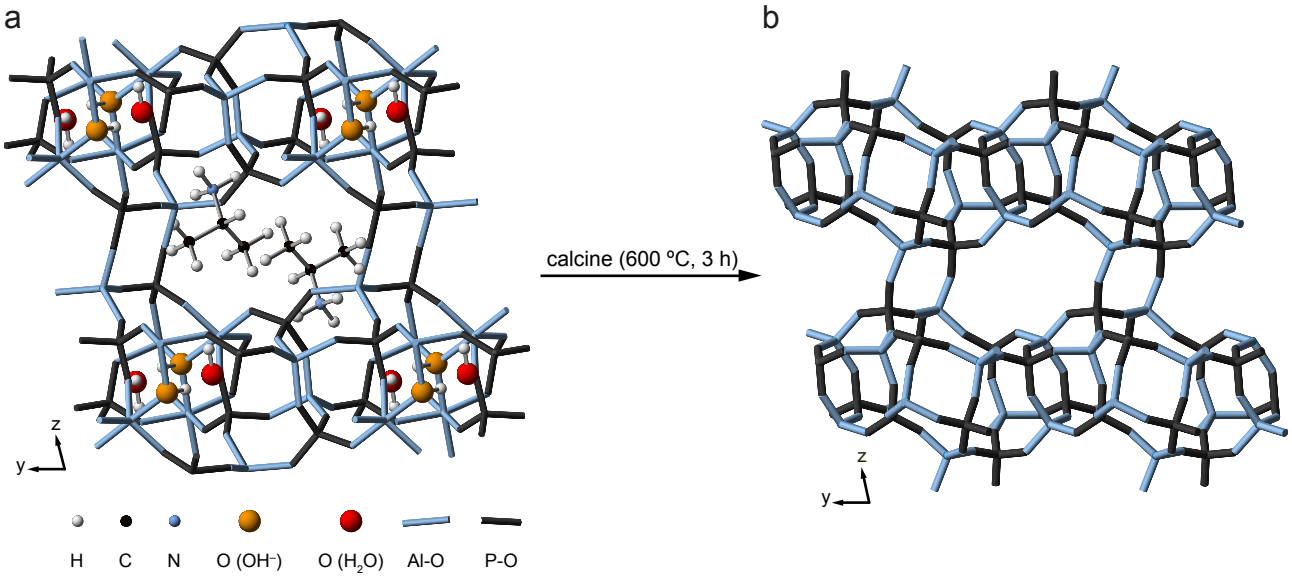

Figure 2

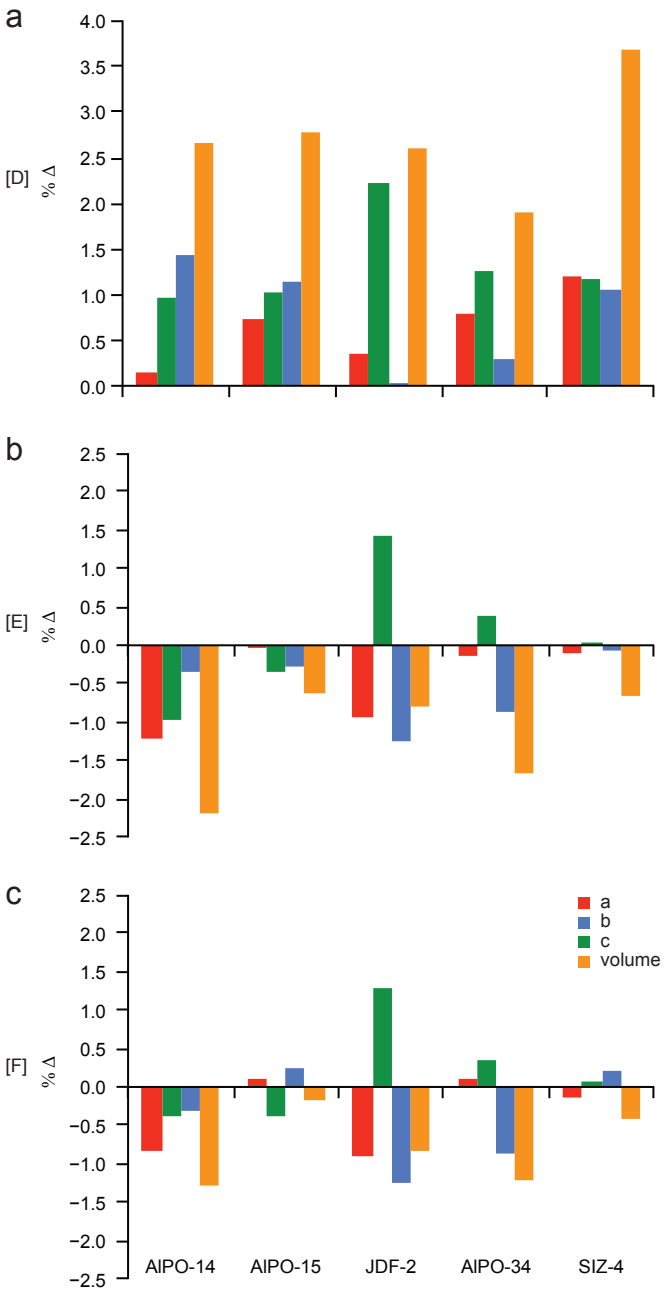
a
[D] % Δ
4.0
3.5
3.0
2.5
2.0
1.5
1.0
0.5
0.0
b
[E] % Δ
2.5
2.0
1.5
1.0
0.5
0.0
−0.5
−1.0
−1.5
−2.0
−2.5
c
[F] % Δ
a
b
c
volume
AlPO-14
AlPO-15
JDF-2
AlPO-34
SIZ-4

Figure 3

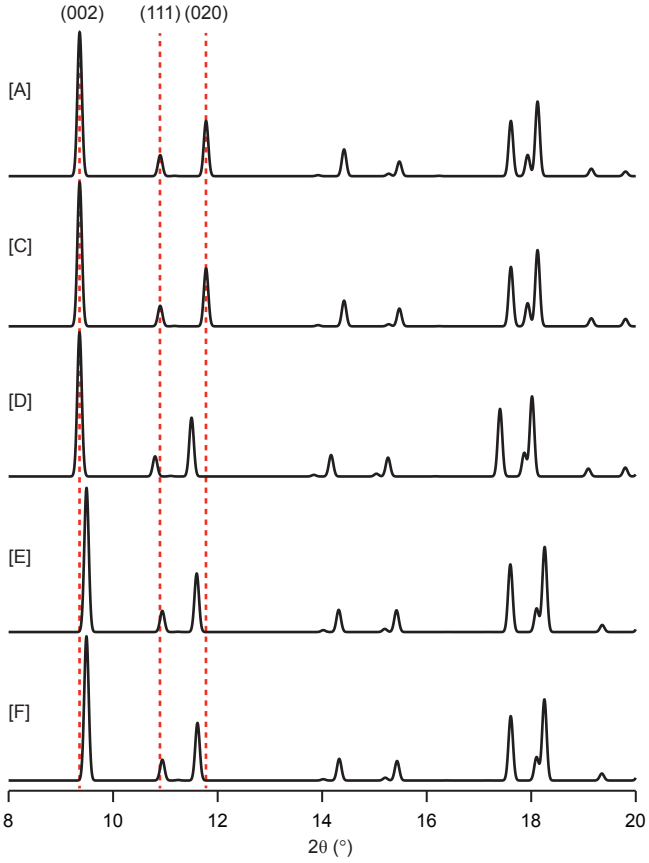

Figure 4

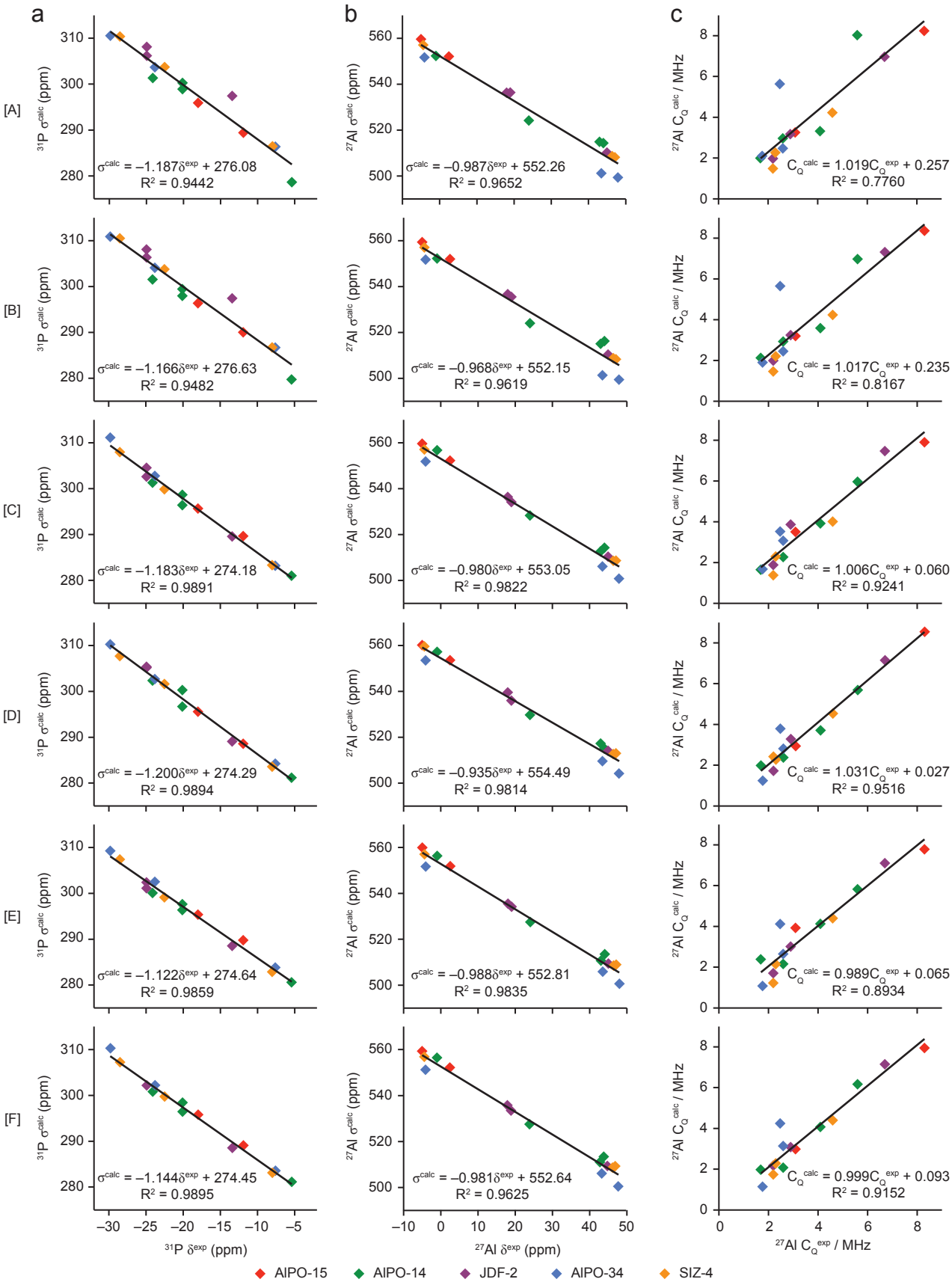
a
b
c
[A]
[B]
[C]
[D]
[E]
[F]
31P σcalc (ppm)
27Al σcalc (ppm)
27Al CQcalc / MHz
σcalc = –1.187δexp + 276.08
R² = 0.9442
σcalc = –0.987δexp + 552.26
R² = 0.9652
CQcalc = 1.019CQexp + 0.257
R² = 0.7760
σcalc = –1.166δexp + 276.63
R² = 0.9482
σcalc = –0.968δexp + 552.15
R² = 0.9619
CQcalc = 1.017CQexp + 0.235
R² = 0.8167
σcalc = –1.183δexp + 274.18
R² = 0.9891
σcalc = –0.980δexp + 553.05
R² = 0.9822
CQcalc = 1.006CQexp + 0.060
R² = 0.9241
σcalc = –1.200δexp + 274.29
R² = 0.9894
σcalc = –0.935δexp + 554.49
R² = 0.9814
CQcalc = 1.031CQexp + 0.027
R² = 0.9516
σcalc = –1.122δexp + 274.64
R² = 0.9859
σcalc = –0.988δexp + 552.81
R² = 0.9835
CQcalc = 0.989CQexp + 0.065
R² = 0.8934
σcalc = –1.144δexp + 274.45
R² = 0.9895
σcalc = –0.981δexp + 552.64
R² = 0.9625
CQcalc = 0.999CQexp + 0.093
R² = 0.9152
31P δexp (ppm)
27Al δexp (ppm)
27Al CQexp / MHz
AlPO-15
AlPO-14
JDF-2
AlPO-34
SIZ-4

Figure 5

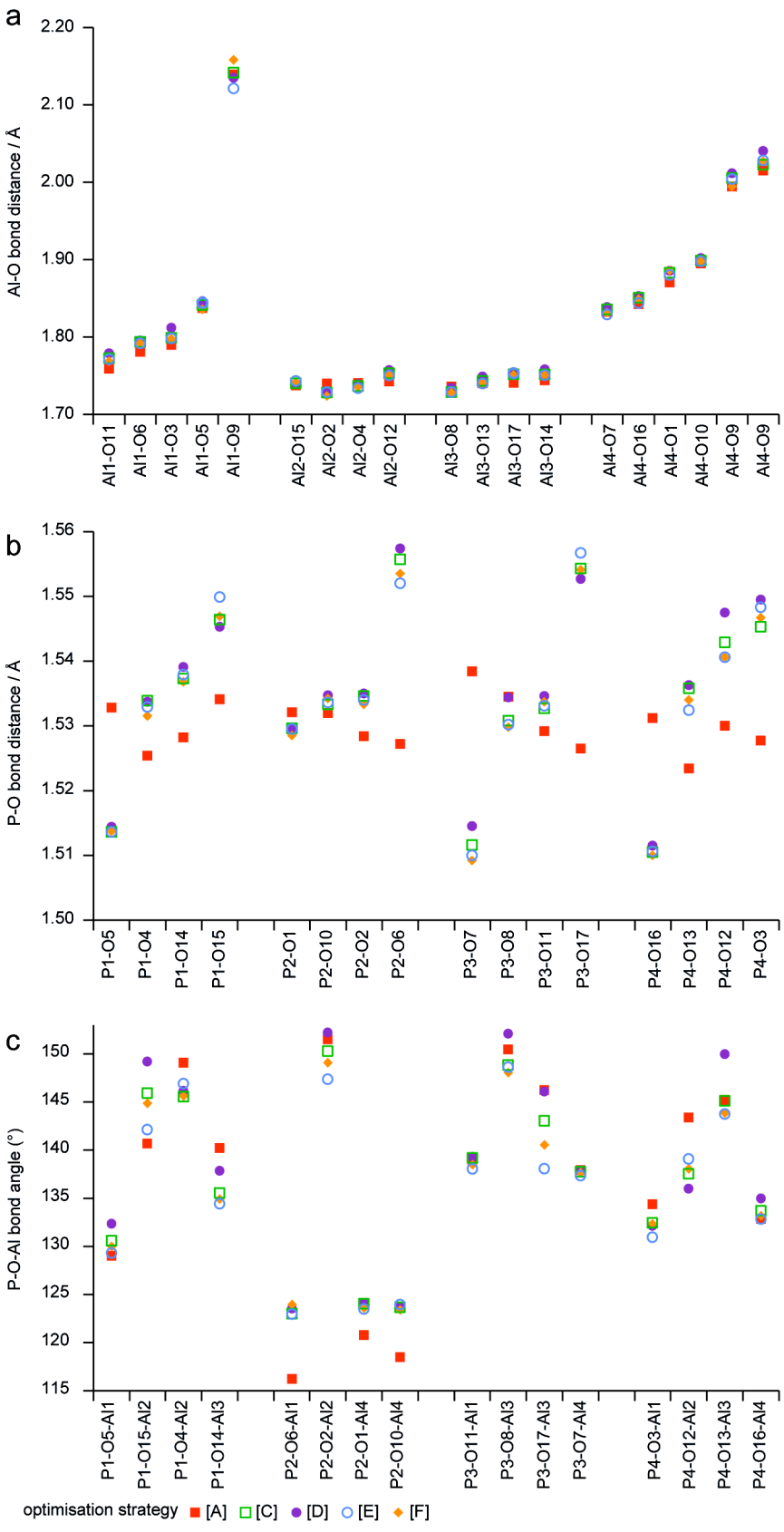
a
Al-O bond distance / Å
2.20
2.10
2.00
1.90
1.80
1.70
Al1-O11
Al1-O6
Al1-O3
Al1-O5
Al1-O9
Al2-O15
Al2-O2
Al2-O4
Al2-O12
Al3-O8
Al3-O13
Al3-O17
Al3-O14
Al4-O7
Al4-O16
Al4-O1
Al4-O10
Al4-O9
Al4-O9
b
P-O bond distance / Å
1.56
1.55
1.54
1.53
1.52
1.51
1.50
P1-O5
P1-O4
P1-O14
P1-O15
P2-O1
P2-O10
P2-O2
P2-O6
P3-O7
P3-O8
P3-O11
P3-O17
P4-O16
P4-O13
P4-O12
P4-O3
c
P-O-Al bond angle (°)
150
145
140
135
130
125
120
115
P1-O5-Al1
P1-O15-Al2
P1-O4-Al2
P1-O14-Al3
P2-O6-Al1
P2-O2-Al2
P2-O1-Al4
P2-O10-Al4
P3-O11-Al1
P3-O8-Al3
P3-O17-Al3
P3-O7-Al4
P4-O3-Al1
P4-O12-Al2
P4-O13-Al3
P4-O16-Al4
optimisation strategy [A] [C] [D] [E] [F]

Figure 6

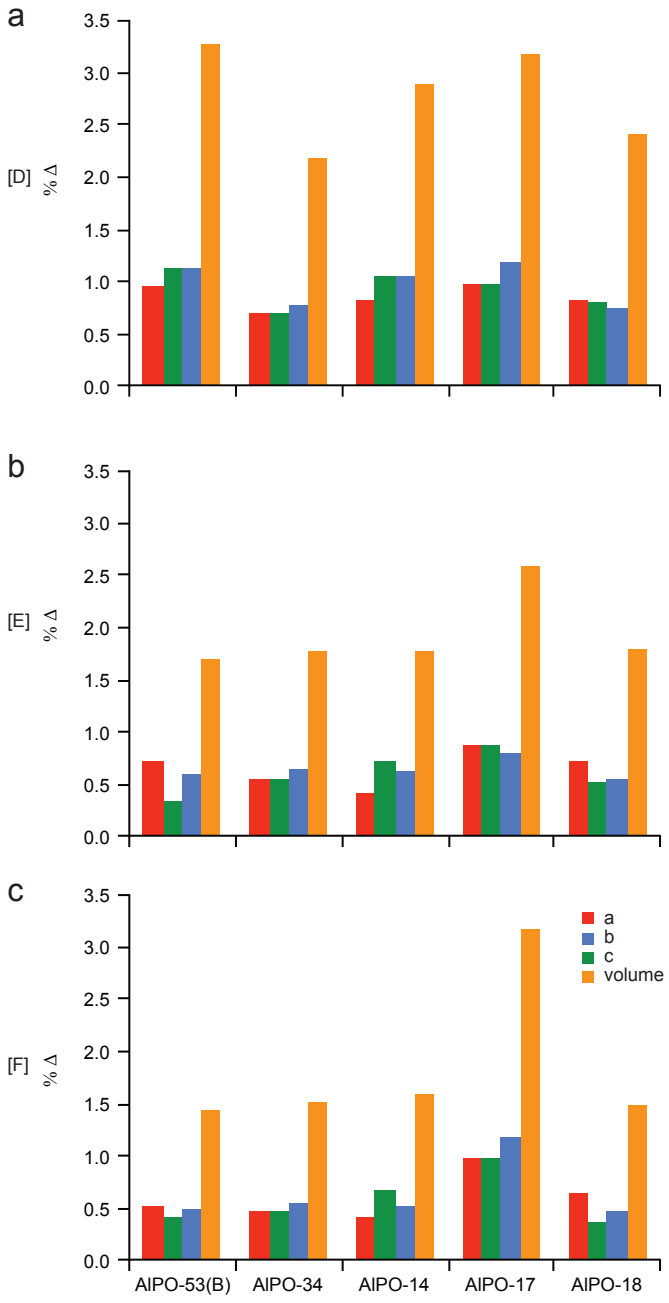
a
b
c
[D] % Δ
[E] % Δ
[F] % Δ
3.5
3.0
2.5
2.0
1.5
1.0
0.5
0.0
a
b
c
volume
AlPO-53(B)
AlPO-34
AlPO-14
AlPO-17
AlPO-18

Figure 7

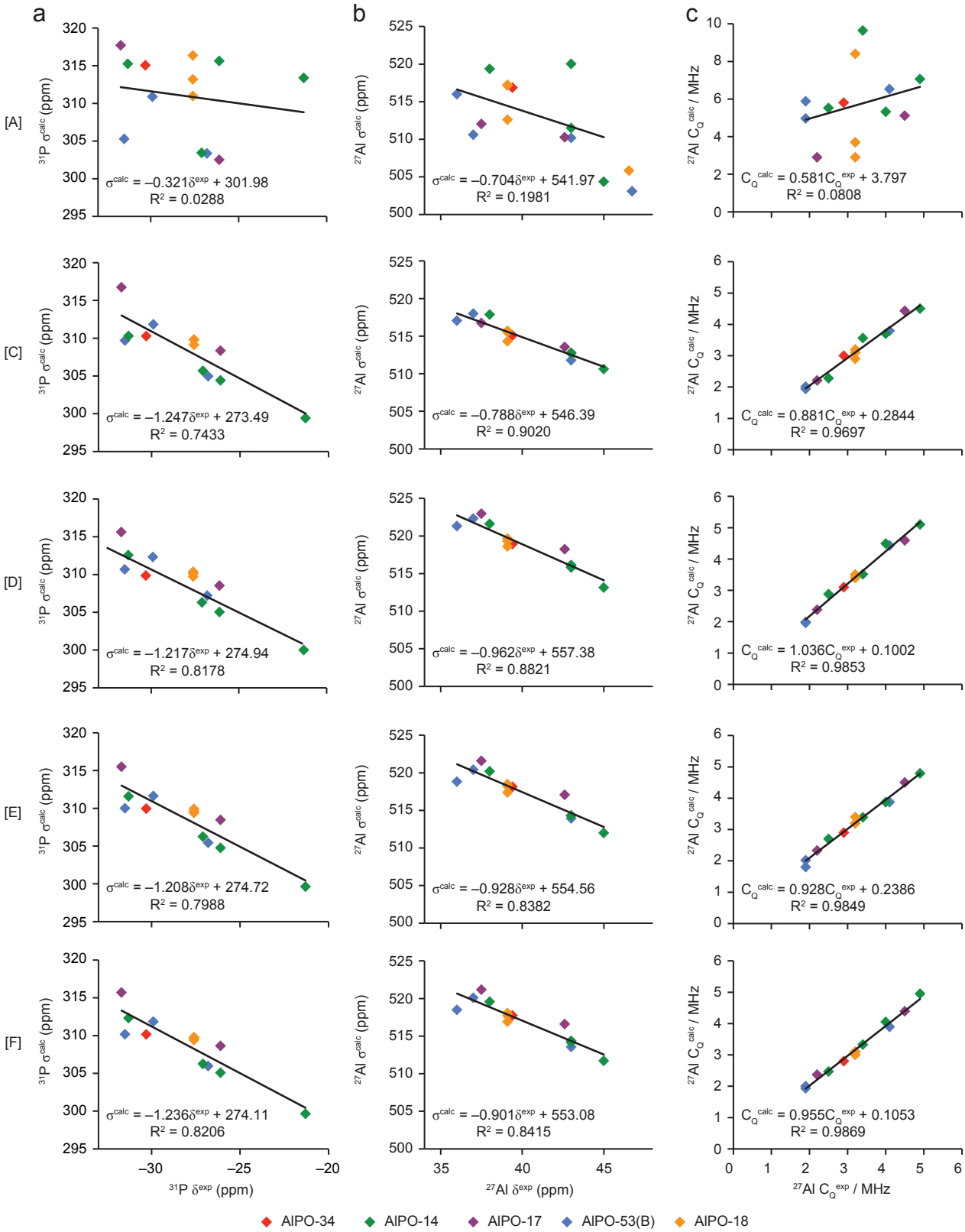
a
b
c
[A]
[C]
[D]
[E]
[F]
^{31}P σ^{calc} (ppm)
^{27}Al σ^{calc} (ppm)
^{27}Al C_Q^{calc} / MHz
$\sigma^{calc} = -0.321\delta^{exp} + 301.98$ $R^2 = 0.0288$
$\sigma^{calc} = -0.704\delta^{exp} + 541.97$ $R^2 = 0.1981$
$C_Q^{calc} = 0.581C_Q^{exp} + 3.797$ $R^2 = 0.0808$
$\sigma^{calc} = -1.247\delta^{exp} + 273.49$ $R^2 = 0.7433$
$\sigma^{calc} = -0.788\delta^{exp} + 546.39$ $R^2 = 0.9020$
$C_Q^{calc} = 0.881C_Q^{exp} + 0.2844$ $R^2 = 0.9697$
$\sigma^{calc} = -1.217\delta^{exp} + 274.94$ $R^2 = 0.8178$
$\sigma^{calc} = -0.962\delta^{exp} + 557.38$ $R^2 = 0.8821$
$C_Q^{calc} = 1.036C_Q^{exp} + 0.1002$ $R^2 = 0.9853$
$\sigma^{calc} = -1.208\delta^{exp} + 274.72$ $R^2 = 0.7988$
$\sigma^{calc} = -0.928\delta^{exp} + 554.56$ $R^2 = 0.8382$
$C_Q^{calc} = 0.928C_Q^{exp} + 0.2386$ $R^2 = 0.9849$
$\sigma^{calc} = -1.236\delta^{exp} + 274.11$ $R^2 = 0.8206$
$\sigma^{calc} = -0.901\delta^{exp} + 553.08$ $R^2 = 0.8415$
$C_Q^{calc} = 0.955C_Q^{exp} + 0.1053$ $R^2 = 0.9869$
^{31}P δ^{exp} (ppm)
^{27}Al δ^{exp} (ppm)
^{27}Al C_Q^{exp} / MHz
AlPO-34
AlPO-14
AlPO-17
AlPO-53(B)
AlPO-18

Figure 8

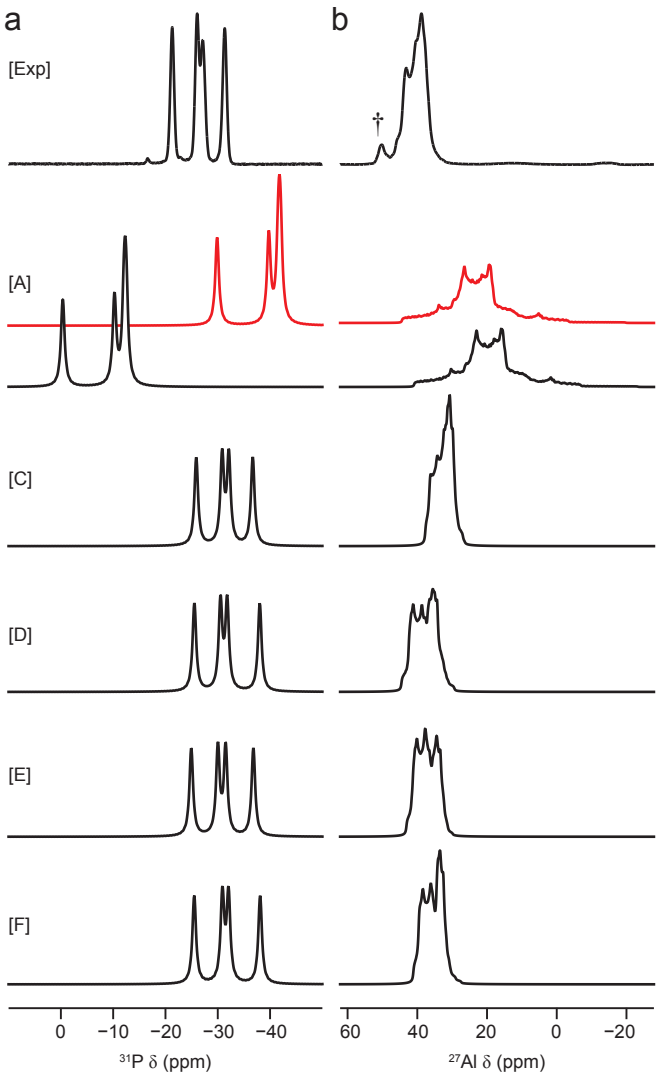

Figure 9

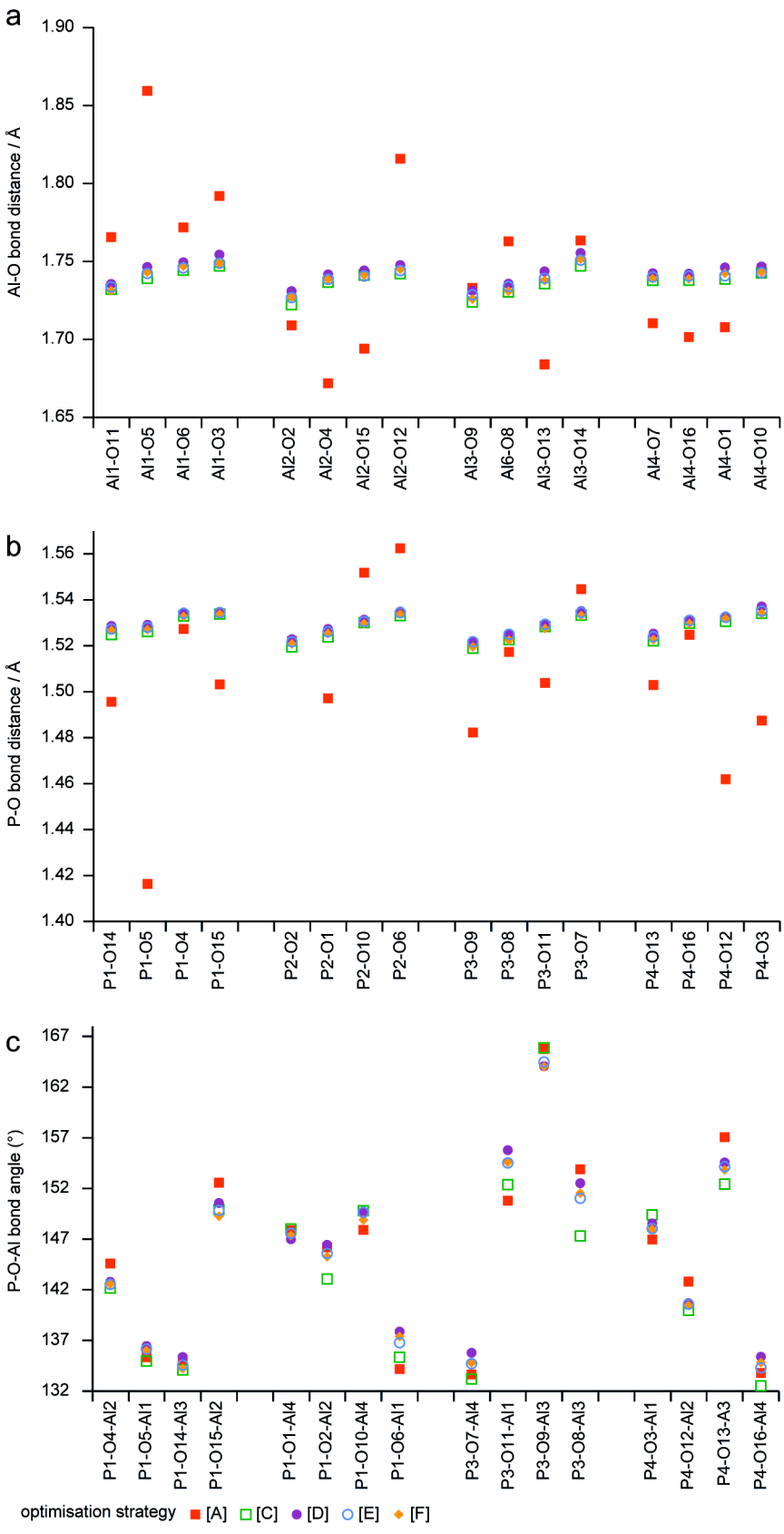
a
Al-O bond distance / Å
1.90
1.85
1.80
1.75
1.70
1.65
Al1-O11
Al1-O5
Al1-O6
Al1-O3
Al2-O2
Al2-O4
Al2-O15
Al2-O12
Al3-O9
Al6-O8
Al3-O13
Al3-O14
Al4-O7
Al4-O16
Al4-O1
Al4-O10
b
P-O bond distance / Å
1.56
1.54
1.52
1.50
1.48
1.46
1.44
1.42
1.40
P1-O14
P1-O5
P1-O4
P1-O15
P2-O2
P2-O1
P2-O10
P2-O6
P3-O9
P3-O8
P3-O11
P3-O7
P4-O13
P4-O16
P4-O12
P4-O3
c
P-O-Al bond angle (°)
167
162
157
152
147
142
137
132
P1-O4-Al2
P1-O5-Al1
P1-O14-Al3
P1-O15-Al2
P1-O1-Al4
P1-O2-Al2
P1-O10-Al4
P1-O6-Al1
P3-O7-Al4
P3-O11-Al1
P3-O9-Al3
P3-O8-Al3
P4-O3-Al1
P4-O12-Al2
P4-O13-A3
P4-O16-Al4
optimisation strategy [A] [C] [D] [E] [F]

TOC Graphic

The use of dispersion-corrected density functional theory methods (DFT-D) for the structural optimisation of aluminophosphate frameworks, and the effect upon the calculated solid-state NMR parameters is investigated.